Review Article
Kinetic modeling in PET imaging of hypoxia

Fan Li[1,2], Jesper T Joergensen[1,2], Anders E Hansen[1,3], Andreas Kjaer[1,2]

[1]Cluster for Molecular Imaging, University of Copenhagen, Blegdamsvej 3, 2200 Copenhagen, Denmark; [2]Department of Clinical Physiology, Nuclear Medicine & PET, Rigshospitalet, University of Copenhagen, Blegdamsvej 9, 2100 Copenhagen, Denmark; [3]Department of Micro- and Nanotechnology, Center for Nanomedicine and Theranostics, DTU Nanotech, Technical University of Denmark, Building 423, 2800 Lyngby, Denmark

Abstract: Tumor hypoxia is associated with increased therapeutic resistance leading to poor treatment outcome. Therefore the ability to detect and quantify intratumoral oxygenation could play an important role in future individual personalized treatment strategies. Positron Emission Tomography (PET) can be used for non-invasive mapping of tissue oxygenation *in vivo* and several hypoxia specific PET tracers have been developed. Evaluation of PET data in the clinic is commonly based on visual assessment together with semiquantitative measurements e.g. standard uptake value (SUV). However, dynamic PET contains additional valuable information on the temporal changes in tracer distribution. Kinetic modeling can be used to extract relevant pharmacokinetic parameters of tracer behavior *in vivo* that reflects relevant physiological processes. In this paper, we review the potential contribution of kinetic analysis for PET imaging of hypoxia.

Introduction

The majority of locally advanced solid tumors exhibit hypoxic and even anoxic regions that are heterogeneously distributed within the tumor mass [1]. These regions are a result of an imbalance between oxygen supply and consumption and can generally be divided into perfusion limited (acute) hypoxia, which is generated by the diffuse nature of tumor vasculature, and diffusion limited (chronic) hypoxia, which develops as the distance between tumor vasculature, and the expanding tumor cells increases. Additionally, cancer associated anemia may contribute to the formation of tumor hypoxia following a decrease in the bloods ability to carry the oxygen [2].

The intricate link between tumor hypoxia and increased malignancy is well established [3-5]. In addition, hypoxic tumor cells represent an important therapeutic problem because of increased resistance towards ionizing radiation and chemotherapy [6-9]. The therapeutic targeting of tumor hypoxia represents an attractive strategy for individualized therapy of cancer patients. In radiation oncology different approaches such as the use of adjuvant hypoxia sensitizers (e.g. nimorazole) during radiation therapy [10, 11]; therapeutic combinations aiming to increase tumor oxygenation [12-14]; and modern high linear energy transfer radiation strategies (e.g. heavy ion therapy) [15] has been applied with varying results. Additionally, heterogeneous delivery of radiation, also termed dose painting, holds the potential to selectively increase radiation dose to areas with known therapeutic resistance, such as hypoxic tumor regions. This approach is extremely challenging, as it requires the ability to continuously identify regional changes in intratumoral oxygenation levels, and currently knowledge is very limited with regard to how regional oxygenation fluctuates during therapy [16, 17]. Therefore methods that allow for identification of patients with hypoxic tumors that would benefit from hypoxia-modified treatment could improve treatment efficacy. However, presently no method has reached a position as a clinically accepted routine approach for identification of tumor hypoxia, even though a number of techniques have been evaluated to deter-
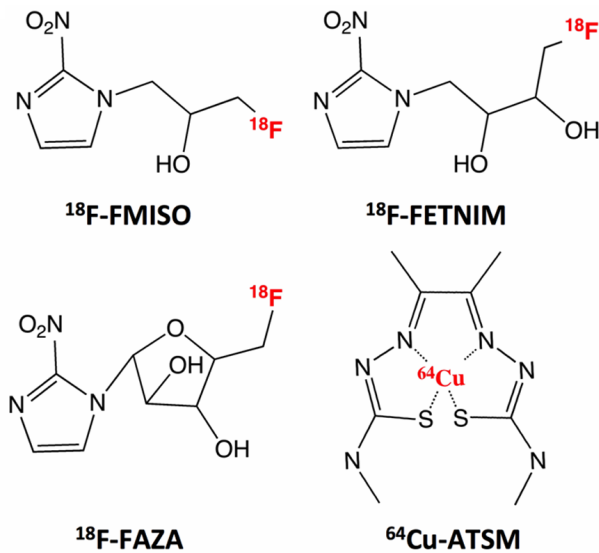
Figure 1. Chemical structures of hypoxia specific PET tracers. ^{18}F-FMISO: ^{18}F-fluoromisonidazole; ^{18}F-FETNIM: ^{18}F-fluoroerythronitroimidazole; ^{18}F-FAZA: ^{18}F-fluoroazomycin; ^{64}Cu-ATSM: [64]Cu(II)diacethyl-bis(N4-methylthiosemicarbazone). Besides ^{64}Cu, Cu-ATSM can also be labeled with other radioactive copper isotopes such as [60]Cu, [61]Cu and [62]Cu.

mine oxygenation in tissue. The polarographic electrode is currently the only method that can provide a direct measure of oxygen tension, and it has been considered as the gold standard for measurement of tumor pO[2] over the last two decades [4, 18-20]. In addition, a different type of electrode based on the principle of oxygen-induced quenching of light emitted by fluorescent dye, has also been used for this purpose [21-23]. Immunohistochemical staining of exogenous or endogenous surrogate markers of hypoxia in tumor biopsies is another approach often used to assess tumor oxygenation [24-26]. However, these needle-based methods have some limitations as they are invasive procedures and only applicable for tumors that are accessible with a needle. Moreover, these techniques only allows for the assessment of oxygenation in a limited volume of the tumor microenvironment. The heterogeneous distribution of hypoxic areas makes a non-invasive imaging approach attractive, and different techniques such as magnetic resonance imaging (MRI) and electron paramagnetic resonance (EPR) with oxygen sensitive probes have been applied for assessment of tumor oxygenation [27-30]. Additionally, positron emission tomography (PET) offers *in vivo* measurement and quantification of physiologi-

cal processes with high temporal and adequate spatial resolution.

At present the radiolabelled glucose analog, 2-deoxy-2-(^{18}F)fluoro-D-glucose (^{18}F-FDG) is the most used PET tracer in clinical oncology. It utilizes that cancer cells take up greatly elevated levels of glucose, known as the Warburg effect [31, 32]. Additionally, ^{18}F-FDG has also been proposed as a surrogate marker of tumor hypoxia following the potential increased cell metabolism from oxidative phosphorylation to glycolysis when oxygen level drops [33]. This induce an increase in the uptake of glucose but despite this well-characterized connection, preclinical and clinical studies have reported conflicting results; but in general ^{18}F-FDG cannot be considered as a consistent surrogate marker of hypoxia in tumors [34-39]. Accordingly, several radiotracers for specific PET imaging of hypoxia including ^{18}F-Fluoromisonidazole ^{18}F-FMISO, fluoroazomycin (^{18}F-FAZA), fluoroerythronitroimidazole (^{18}F-FETNIM) and copper(II)diacethyl-bis(N4-methylthiosemicarbazone) (Cu-ATSM) have been developed (**Figure 1**).

One of the advantages of PET is the ability to measure radiotracer concentration in tissue or organs. Semiquantitative approaches are often used for analysis of PET images but the main drawback is that it does not take into account variations caused by underlying processes such as tracer delivery, trapping, competition with other molecules, and physical clearance [40]. Dynamic PET can be used to study tracer pharmacokinetics and temporal changes in uptake, and clinical studies have indicated that valuable additional information can be obtained from the profile of time activity curves (TACs) [32, 41, 42]. Furthermore, mathematical modeling based on non-invasive imaging data can possibly be used to extract meaningful parameters of tracer accumulation and distribution kinetics [40, 43-46].

Basically, tracer kinetic modeling is based on a compartmental model that is comprised of a number of functional, homogenous units termed compartments. These are interpreted as separate, structureless pools of tracer in distinct state. The tracer transport between compartments can be described by rate param-
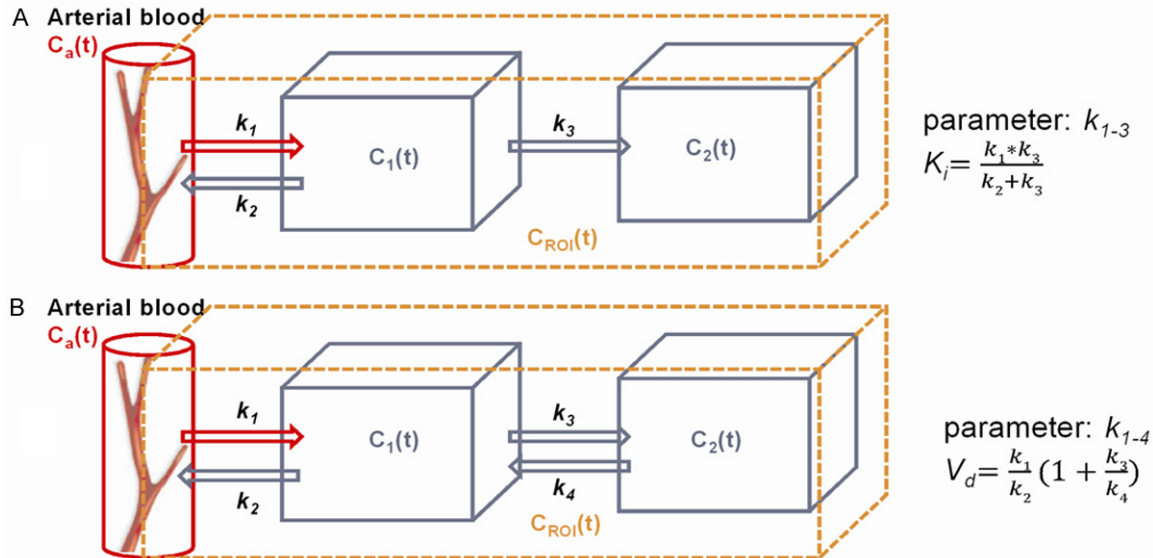
Figure 2. Graphical representation of common 2-tissue compartment models. Model (A) is consisting of three components and each is a function of time expressed as time activity curves. Input function, $C_a(t)$ consists primarily of arterial blood and interstitial space close to vessels. The $C_1(t)$ compartment represents unbound tracer in tissue whereas $C_2(t)$ compartment represents bound tracer. This model contains three kinetic parameters, k_{1-3}. Model (B) contains the same number of compartments but kinetic parameter also includes the transport rate constant k_4. Moreover, the netto influx parameter, K_i can be calculated based on k_{1-3} in a irreversible model, and k_{1-4} can be used to calculate the distribution volume, V_d in a reversible model.

eters, and usually the models are described mathematically by first order differential equations. **Figure 2** demonstrates the two most widely used model structures within tracer kinetic studies. While a 2-tissue reversible model is often applied in studies of neuroreceptor-ligands, a 2-tissue irreversible model has been implemented in most studies of hypoxia tracer kinetics [47, 48]. In principle, additional compartments can be added to a model in order to obtain a more realistic interpretation of tracer kinetic behavior *in vivo,* including an increasing number of parameters. However, increased complexity affects the accuracy and reliability of the model parameter estimation due to limitation of the nonlinear minimization problem [49]. Therefore model selection should be considered as a balance between statistical accuracy and model complexity. As an alternative, graphical analysis is a more computational efficient way to calculate combinatorial parameters by turning a nonlinear problem into linear plots [50]. Thus the slope of the linear part of Patlak and Logan plots can be used to determine netto influx rate, K_i and distribution volume, V_d for tracers with irreversible and reversible uptake, respectively.

Overall compartmental analysis provides a possibility to understand the tracer behavior in a specific tissue and allows for the derivation of important kinetic parameters. This can provide additional information on a metabolic processes at the molecular level and thereby potentially improve the diagnostic and prognostic potential of a PET tracer. This review focuses on studies where compartment/kinetic modeling has been applied on PET data for quantification of hypoxia.

^{18}F-FMISO

The majority of hypoxia PET tracers belongs to a group of compounds termed nitroimidazoles that have been used intensively as immunological markers for immunohistochemical procedures and flowcytometry [51-55]. Nitroimidazoles enter cells by diffusion and are reduced by nitroreductases inversely correlated with oxygen tension. In the presence of oxygen they are able to leave the cell again, but under hypoxic conditions the nitroimidazoles become reduced and will be irreversibly trapped within the cells [56, 57].

[18]F-Fluoromisonidazole (^{18}F-FMISO) was the first nitroimidazole-based radiotracers for
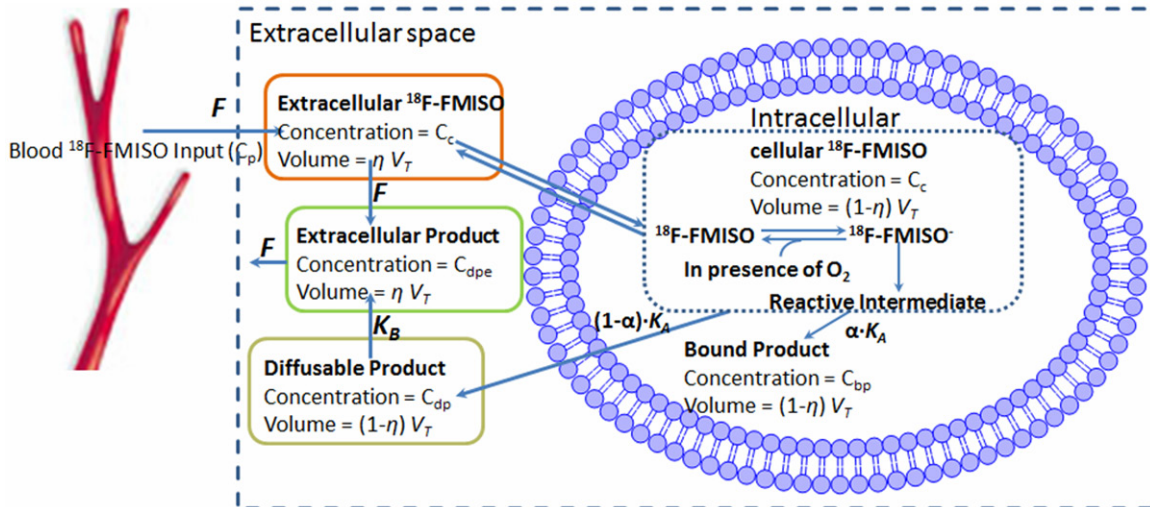
Figure 3. The model of ^{18}F-FMISO transport and metabolism presented by Casciari *et al*. ^{18}F-FMISO enters the target tissue by flood flow (*F*) and diffuse across the cell membrane, where it is reduced. K_A is the rate constant describing the rate by which FMISO is reduced. Cellular accumulation of FMISO and washout of diffusible product is running side by side. C_c, C_p, C_{bp}, C_{dp}, C_{dpe} corresponds to ^{18}F-FMISO concentration in tissue, in blood plasma, ^{18}F-FMISO bound product and cellular diffusible product, respectively. V_T, η are the tissue specific volume and dimensionless fractional variable. K_A is related to the oxygen level and can be considered as a surrogate measure of hypoxia.

hypoxia PET imaging to be developed, and it has been extensively used in both preclinical and clinical studies [58-63].

The kinetic profile and characteristics of ^{18}F-FMISO has also been investigated in a number of studies applying various approaches. In 1995 Casciari *et al*. developed a mathematical model based on knowledge on the cellular metabolism and tracer transport in tissue. The main objective was to quantify ^{18}F-FMISO reaction rate constant, K_A, a parameter related to the level of cellular oxygen (see **Figure 3**). Models performance was tested using Monte Carlo simulation and fitted to ^{18}F-FMISO time-activity PET data from human and rat tumors. This demonstrated the importance of including some transport limits such as parameter fixing of the compartments representing tracer in the tissue. In addition the effect of noise on accurately determination of K_A was small when some parameters were fixed at physiological meaningful values; however, the accuracy of K_A was sensitive to the accuracy of the fixed parameters [64].

Kelly and Brady also did a simulation work on the spatiotemporal distribution of ^{18}F-FMISO in tumor microenvironment by applying a modular approach to simulated data. They included parameters to model spatial diffusion of free

^{18}F-FMISO and its reduced compounds and modified a conversional reversible 2-compartmental model, with a reaction-diffusion equation, in order to improve ^{18}F-FMISO distribution dynamics [65]. The model was then used to generate simulated data based on patient plasma time activity curve as input. It was necessary to set transport parameter k_4 = 0. Additionally, a number of technical limitations that influenced the model were identified. On the basis on this, the kinetic and spatial effects of diffusion could be disregarded in the data fitting process. The adaptive model illustrated that a reversible 2-compartment model with varying diffusion distances and diffusion coefficients was able to generate more realistic TACs. Moreover, it demonstrated that simulation models of tracer spatiotemporal distributions provides a options to investigate the effects of heterogeneity on TACs and the relationships between image data and molecular processes, prior to empirical studies.

Besides these simulation studies of ^{18}F-FMISO, a limited number of preclinical studies in mice and rats have focused on kinetic modeling. Whisenant *et al*. did a study in nude mice bearing Trastuzumab-resistant breast tumors in order to test the reproducibility of kinetic parameters derived from dynamic PET scan protocols [66]. Mice received 60 min dynamic

PET scan six hours apart with ^{18}F-FLT and ^{18}F-FMISO, respectively. They found that the distribution volume, V_d and the net influx constant, K_i were the most reproducible parameters for ^{18}F-FMISO. In contrast transport constant k_1 and trapping constant k_3 were the most variable. For ^{18}F-FLT V_d, k_3, and K_i were shown to be the most reproducible parameters.

In another study Bejot *et al.* evaluated ^{18}F-3-NTR, a 3-nitro-1,2,4-triazole analogue (N(1) substituted) (^{18}F-3-NTR) against ^{18}F-FMISO as hypoxia PET tracer in tumor bearing mice and concluded that ^{18}F-3-NTR could not be considered a hypoxia imaging agent due to its poor binding capacity [67]. Furthermore, based on the Akaiki information criterion there was no benefit of applying a 3-compartment irreversible model to describe ^{18}F-FMISO kinetics when compared to a 2-compartment irreversible model.

In a recent study, Bartlett *et al.* investigated a group of nude rats bearing prostate tumors in order to find a non-invasive approach based on dynamic PET for better identification of tumor hypoxia [23]. Voxelwise kinetic parameters calculated from 2-compartment model fitting to ^{18}F-FMISO uptake data were compared to pO_2 measurements. When k_1 and k_2 were constrained, ^{18}F-FMISO trapping rate, k_3 was shown to be a more robust discriminator for low pO_2 within tumor tissue than a simple tissue-to-plasma ratio. This suggest that voxelwise based kinetic modeling could improve accuracy of tumor hypoxia estimation.

Finally, the use of kinetic modeling of ^{18}F-FMISO has also been investigated in a few clinical studies. Bruehlmeier *et al.* used ^{15}O-H$_2$O to study the influence of perfusion on the pharmacokinetics of ^{18}F-FMISO in eleven patients with brain cancer and observed an increased late uptake in glioblastomas [68]. Pixel-wise comparison showed a positive relationship between ^{15}O-H$_2$O and early uptake of ^{18}F-FMISO, whereas no correlation was found for late ^{18}F-FMISO distribution. Standard 2- and 3-compartment models and Logan graphical analysis were used to calculate distribution volumes and transport rate constants and found that a V_d above one was indicative of active ^{18}F-FMISO uptake. Additionally, the ^{18}F-FMISO uptake rate, k_1 was increased in all tumor tissue, compared to values in white matter and in cortex. In

meningioma they found the highest value for k_1 of all brain tumors. This increase k_1 permitted delineation of the meningioma in an early ^{18}F-FMISO PET image, but the tumor did not exhibit subsequent ^{18}F-FMISO accumulation and was not visualized in the late PET images. Accordingly, the ^{18}F-FMISO distribution volume in the meningioma was not increased despite a high k_1 value. However, despite V_d providing a good measure of ^{18}F-FMISO accumulation, it was concluded that it does not offer additional information compared to tumor-to-background ratios of late PET images.

Using a similar experimental setup with ^{15}O-H$_2$O and ^{18}F-FMISO, Bruehlmeier *et al.* applied graphical analysis on dynamic PET data from six dogs with spontaneous sarcomas [69]. They found that tumor tissue could be markedly delineated from surrounding tissue including muscles by positive influx rate K_i derived from a Patlak plot. The presence of tumor hypoxia was confirmed by eppendorf electrode measurement.

In a study of head and neck cancer patients, Thorwarth *et al.* performed quantitative image analysis based on irreversible compartmental modeling of dynamic ^{18}F-FMISO PET data [70]. This model was different from previous approaches by including weighing factors for the respective model compartments. The input function was determined from the signal of a reference tissue and the irreversible model was applied to identify and quantify TACs using a voxel-to-voxel approach. Evaluation of model performance indicated that the parameters derived from the kinetic model were superior to SUV for quantification in extremely low oxygenated and necrotic tissue areas. In another study the same model was applied to a small group of head and neck cancer patients that were scanned dynamically for 60 min prior to radiotherapy [42]. Assessment parameters representing hypoxia and perfusion derived from the kinetic model were not able to predict treatment outcome. However, Thorwarth *et al.* introduced a novel parameter, termed the malignancy value, that was dependent on both hypoxia and perfusion characteristics of the tissue. This malignancy value could be used as a prognostic factor indicating that the parameters may provide additive information. Furthermore, in a preclinical study, Cho *et al.* adapted Thorwarth's model for comparing perfusion

and hypoxia parameters derived from MRI with ^{18}F-FMISO PET in a rat prostate cancer model [71]. The tumor perfusion derived from DCE-MRI was found positively correlated with early ^{18}F-FMISO PET but inversely correlated to late slope maps of the ^{18}F-FMISO PET time-activity curve.

Wang *et al.* applied a generic irreversible 2-compartmental model to analyze dynamic ^{18}F-FMISO PET dataset within three regions of an image phantom [72]. The purpose of the phantom study was to determine the statistical accuracy and precision of the kinetic analysis. The results from the phantom study was used for guidance in a clinical dynamic ^{18}F-FMISO PET study of nine head and neck cancer patients with local squamous cell carcinoma [73]. Based on this they identified K_i as a potential hypoxia marker and found a significant correlation to ^{18}F-FMISO tumor-to-blood ratio.

In addition to modeling of tumor hypoxia, ^{18}F-FMISO has also been used in studies of ischemic stroke. Takasawa *et al.* performed a rat stoke study that included dynamic PET with ^{18}F-FMISO. In order to obtain quantitative comparison between the tracer retention from affected and unaffected cerebral hemispheres, an irreversible compartmental model was used for calculation of k_1 and K_i [74]. Immediately after the occlusion of the middle cerebral artery a remarkable increased K_i was observed in the affected site. This suggests that ^{18}F-FMISO can potentially be used to visualize the occlusion at a very early stage. However, in spite of histological findings, no difference in either k_1 and K_i was found between affected and unaffected cerebral hemispheres 48 hours after the occlusion. In another study Hong *et al.* used the dataset generated by Takasawa *et al.* to perform kinetic analysis [75]. Basis functions from plasma input compartment (BAFPIC) model is a modified version of the standard compartment model approach and can be applied to both reversible and irreversible models. In this study BAFPIC was compared to both conventional compartment modeling, as well as the most common analysis methods for generation of parametric maps. The BAFPIC method showed lower variability and bias than nonlinear least squares modeling in hypoxic tissue. In addition, voxel based parametric mapping of dynamic imaging was shown to be less affected by noise-induced variability compared to nonlin-ear least squares modeling and Patlak graphical analysis. BAFPIC could therefore potentially be applied to other tracers with irreversible characteristics, and although the focus of this study was on voxelwise modeling, other kinetic parameter estimations in regions with noise can be performed using the BAFPIC algorithm as well.

^{18}F-FETNIM

Even though ^{18}F-FMISO has been used extensively, a slow hypoxia specific retention and clearance from non-hypoxic tissue is a limitation and results in low tumor-to-background contrast [76]. To improve image quality ^{18}F-labeled nitroimidazole analogs including ^{18}F-FETNIM, 2-nitroimidazole nucleoside analog (^{18}F-HX4) and 2-(2-Nitromidazole-1H-yl)-N-(2,2,3,3,3-pentafluoropropyl)acetamind (^{18}F-EF5), that have structural modifications - with changed lipophilic properties, have been developed to overcome the basic pharmacokinetic limitations [44, 77, 78]. ^{18}F-FETNIM was introduced as a novel hypoxia-specific PET tracer in 1995 and has shown promising results in clinical studies [77, 79].

In studies in patients with head and neck cancer Lehtiö *et al.* performed compartmental analysis based on dynamic ^{18}F-FETNIM PET scans [80, 81]. They adapted the model previously introduced by Casciari *et al.* for ^{18}F-FMISO metabolism and transport (**Figure 3**). Blood flow rate (F), tissue activity correction factors ($\beta1$, $\beta2$) and cellular ^{18}F-FETNIM reaction rate (K_A), considered the hypoxia specific binding rate, were estimated by fitting the model to dynamic PET data. They found that the level of tracer uptake (K_A) was most sensitive to changes in oxygen in tissue with high blood flow. Furthermore, distribution volumes derived from Logan plots correlated positively with the tumor-to-plasma ratio but not with tumor-to-muscle ratio. This suggests that plasma should be preferred as reference tissue rather than muscle.

^{18}F-FAZA

Like ^{18}F-FETNIM, ^{18}F-FAZA is a next generation nitroimidazole-based PET tracer. Several studies have compared the tracer kinetics of ^{18}F-FAZA with ^{18}F-FMISO and reported of improvements in washout from non-hypoxic tis-

sue and faster renal clearance [82-84]. Moreover, a recent study of 50 patients confirmed the feasibility of using FAZA PET for detection of tumor hypoxia in clinic [85].

A few studies have focused on kinetic modeling of dynamic ^{18}F-FAZA PET. Reischl et al. demonstrated an increased tumor to blood ratio due to faster vascular clearance of ^{18}F-FAZA when compared to ^{18}F-FMISO and that is one of most important criteria for hypoxia tracer development in relation to hypoxia imaging optimization [86].

Busk et al. reported a dynamic ^{18}F-FAZA animal study in three tumor xenograft models of squamous cell carcinomas of the cervix. The dynamic data were analyzed by an irreversible 2-compartmental model. Overall variations in the pattern of TACs were tumor type dependent. The influx rate constant K_i was shown to have a strong correlation to late ^{18}F-FAZA uptake in two of three tumors models. On the other hand, weak correlation between irreversible parameter k_3 and late ^{18}F-FAZA uptake was observed in two of three tumor models [87].

Two small clinical studies have used dynamic ^{18}F-FAZA PET data to compare different kinetic models. While Shi et al. used a voxelvise approach to correlate model parameters of interest with perfusion measured by ^{15}O-H$_2$O PET in patients with head and neck cancer; Verwer et al. applied the Akaiki information criterion to evaluate model fitting to TACs obtained from nine non-small cell lung cancer patients [88, 89]. Both studies concluded that a reversible 2-compartment model showed the best correlation and robustness with their expectations and assumptions.

Cu-ATSM

Beside the nitromidazole-based compounds, a copper labeled metallocomplex termed copper(II)diacethyl-bis(N4-methylthiosemicarbazone) (Cu-ATSM) has been applied as radiotracer for PET imaging of tumor hypoxia [90]. Image quality is generally superior to the nitroimidazoles, however, despite promising clinical performance [91-93], preclinical data from experimental hypoxia imaging is conflicting with regard to tracer selectivity [94-97]. The mechanism of tracer uptake and retention is still not fully understood but it is believed that Cu(II)-

ATSM is reduced to the unstable [Cu(I)- ATSM]$^-$ complex in both hypoxic and normoxic cells. Under normoxic conditions [Cu(I)-ATSM]$^-$ is reoxidized and thereby able to of leave the cell. The reoxidation of [Cu(I)-ATSM]$^-$ is, however, not expected to occur under hypoxic conditions, and the electrochemically negative molecule becomes irreversibly trapped and dissociates [98, 99].

As for the other hypoxia PET tracers there are only limited data concerning the pharmacokinetics of Cu-ATSM. A simulation work carried out by Holland et al. applied a model based on an in vitro study on cellular uptake and retention of ^{64}Cu-ATSM in EMT6 murine carcinoma cells. The model demonstrated that a decrease in cellular pH may protonate the unstable Cu(I)-ATSM complex and increase the rate of dissociation [100]. The kinetic analysis was consistent with experimental cellular uptake.

Bowen et al. suggested an electrochemical models based on the retention mechanisms for ^{18}F-FMISO and ^{61}Cu-ATSM, respectively [101]. In this work the preclinical data were compared to transformation functions derived from tracer uptake and pO$_2$ measurements. Comparisons between ^{61}Cu-ATSM and ^{18}F-FMISO uptake showed inconsistent results, but this could be due to the different retention mechanisms. However, the results suggested that ^{18}F-FMISO uptake was superior for differentiation of a wide range of pO$_2$ values, but ^{61}Cu-ATSM uptake provided more reliable information on variations at low pO$_2$ range.

In another study Dalah et al. performed a simulation work based on the model adapted from Kelly and Brady [102]. This refined model was used to simulate realistic TACs that were comparable to ^{64}Cu-ATSM patient TACs and showed favorable tumor delineation in form of higher tumor to blood ratio compared to ^{18}F-FMISO.

Kinetic modeling of Cu-ATSM PET has also been applied in a few animal studies. Lewis et al. evaluated Cu-ATSM retention in canine models of hypoxic myocardium [97]. Monoexponential analysis and 2-compartmental model fitting were applied to the TACs in order to determinate washout of Cu-ATSM from regions of the myocardium. Based on the assumption that the relationship between washout and retention is inverse proportional, they reported

of an increase of Cu-ATSM retention in ischemic regions when compared to normal myocardium. Moreover, the data also indicated that Cu-ATSM retention in hypoxic regions of the myocardium was independent of increased perfusion and that there was no retention in necrotic tissue.

Recently, McCall *et al*. performed a preclinical study of ^{64}Cu-ATSM uptake in rats bearing FaDu human head and neck cancer xenografts. Graphical analyses were used to derive the net influx parameter, K_i and distribution volume, V_d. In general, a stronger linear relationship was found for Logan plots but both parameters were significantly higher in tumor tissue when compared to muscle tissue. Additionally, a continuous increasing tumor-to-muscle ratio was observed [103].

Finally, Cu-ATSM has been used in multitracer PET studies where two or three tracers were administered with delayed injections. Following image separation, signal recovery was performed based on differences in tracer kinetics and physical decay. In a phantom study of [62]Cu-ATSM and the perfusion PET tracer, [62]Copper-pyruvaldehyde-bis[N4-methylthiosemicarbazone] ([62]Cu-PTSM), Rust *et al*. demonstrated a great similarity between perfusion and hypoxia parameters obtained by the dual tracer approach, and parameters estimated by single-tracer imaging [104]. The results were later confirmed by Black *et al*. that adapted the phantom study protocol and used it for [62]Cu-ATSM and [62]Cu-PTSM PET imaging in dogs with spontaneous tumors [105]. Rate constants obtained from irreversible 2-compartment modeling was used to evaluate the signal separation of the two PET tracers. However, while k_1 and k_2 could be recovered from the mixed PET signal the recovery of k_3 was more problematic. The same group has also experimented with a triple-tracers setup including ^{18}F-FDG [106]. Altogether, the multitracer approach can potential provide different functional information about physiological processes within a short period of time; thereby decreasing the possible effect of microenvironmental changes. However, there are some questions there needs to be address with regard to the long dynamic acquisition time, and the risk of losing information as a consequence of temporal overlap.

Table 1 summaries studies on kinetic modeling of hypoxia using PET tracers.

Challenges in kinetic modeling of hypoxia PET tracers

Studies on kinetic modeling of hypoxia PET tracer needs also deal with the issues, related to acquisition of dynamic PET data in general. The amplitude of noise can be influenced by several physical factors such as the radiopharmaceutical properties of the tracer, injected dose, frame duration, and the sensitivity of the PET camera. In addition, the size of the volumes of interest (VOI) or voxels will also have effect on the scale of noise. In quantitative analysis of dynamic PET data, the accuracy of kinetic parameter estimation is not only related to the signal to noise ratio, but also the number of model parameters and selection of estimation method [107].

Non-linear least square optimization is the most widely used technique to perform curve-fitting for parameter estimation in conventional compartment modeling [8, 25, 26]. The accuracy of both curve-fitting and determination of particular parameters is sensitive to selection of initial conditions [108]. If the initial conditions are improper, it becomes problematic to find a global minimum of the residual sum of squares for parameters in a multidimensional fitting space [49, 109, 110]. A rational way to obtain initial conditions is by applying parameter estimates from similar tracer kinetic studies. Likewise, species and organ dependent physiological measurements found in literature can be used to define the range for parameter boundaries. If no initial conditions are available simulation or phantom studies can be used to determine approximate values that can be used for model optimization. In addition, a number of linearizing methods can be applied to reduce computational time at the cost of limited model parameter as output [50]. Basis function and generalized linear least squares method are other options that reduce the processing time of parameter estimation compared to nonlinear least-squares approach [59, 111].

The input function has great impact on the model performance, and robust determination is crucial for the accuracy of parameter calculation [112, 113]. The input function is defined as

Table 1. Overview of kinetic modeling work with regard to hypoxia using different hypoxia PET tracers

Tracer	Image Targeting	Methods	Application	Species	Authors
^{18}F-FMISO	Hypoxia	Voxelwise kinetic modeling	Oncology/Prostate tumor	Rat	Bartlett et al. [23]
		Noninvasive pO$_2$ measurement			
^{18}F-FMISO	-	Kinetic model	Oncology	Rat	Casciari et al. [64]
^{3}H-FMISO		Monte Carlo simulations		Patient	
^{18}F-FMISO	Hypoxia, perfusion	Dynamic PET	Oncology/Brain tumor	Patient	Bruehlmeier et al. [68]
^{15}O-H$_2$O		Kinetic models			
		Logan graphical analysis			
^{18}F-FMISO	Hypoxia, perfusion	Patlak graphical analysis	Oncology/Spontaneous sarcomas	Dog	Bruehlmeier et al. [69]
^{15}O-H$_2$O					
^{18}F-FMISO	Hypoxia	Modular simulation	Oncology/Model evaluation	Simulation work	Kelly and Brady et al. [65]
		Probability density function			
^{18}F-FMISO	Hypoxia	Kinetic model	Oncology/Model evaluation	Phantom study	Wang et al. [72]
^{18}F-FMISO	Hypoxia	Pharmacokinetic analysis	Oncology/Head and neck cancer	Patient	Wang et al. [73]
		Dynamic PET/CT			
^{18}F-FMISO	Hypoxia, perfusion	Dynamic PET	Oncology/Head and neck cancer	Patient	Thorwarth et al. [70]
		Two compartment model			
^{18}F-FMISO	Hypoxia	Dynamic PET	Oncology/Radiotherapy	Patient	Thorwarth et al. [42]
		Two compartment model			
^{18}F-FMISO	Hypoxia	DCE-MRI	Oncology/Prostate tumor	Rat	Cho et al. [71]
		Dynamic PET			
		Autoradiography			
^{18}F-FMISO	Hypoxia	Dynamic PET	Oncology/Non-immunogenic carcinoma	Mouse	Bejot et al. [67]
^{18}F-3-NTR		Compartment modeling			
^{18}F-FMISO	Hypoxia	Dynamic PET	Scan protocol validation	Mouse	Whisenant et al. [66]
^{18}F-FDG		Graphical analysis			
^{18}F-FDG		Graphical analysis			
^{18}F-FMISO	Stroke	Dynamic PET	Stroke	Rat	Takasawa et al. [74]
^{18}F-FMISO	Hypoxia	Dynamic PET	Stroke	Rat	Hong et al. [75]
		Voxelwise Kinetic analysis based on basis function method			
^{18}F-FETMIN	Hypoxia	Dynamic PET	Oncology/Head and neck cancer	Patient	Lehtio et al. [80]
		Tumor to plasma ratio			
		Tumor to plasma ratio			
^{18}F-FETMIN	Hypoxia	Dynamic PET	Oncology/Head and neck cancer	Patient	Lehtio et al. [81]
		Compartment analysis			

Tracer	Target	Method	Application	Subject	Reference
^{18}F-FAZA	Hypoxia	Dynamic PET	Oncology/Squamous cell carcinoma	Mouse	Busk *et al.* [87]
		Immunohistochemical staining			
		Immunohistochemical staining			
^{18}F-FAZA	Hypoxia, perfusion	Dynamic PET	Oncology/Head and neck cancer	Patient	Shi *et al.* [88]
^{15}O-H$_2$O		Kinetic model			
^{18}F-FAZA	Hypoxia	Dynamic PET/CT	Oncology/No-small cell lung cancer	Patient	Verwer *et al.* [89]
^{60}Cu-ATSM	Hypoxia	Compartment analysis	Myocardial ischemia	Dog	Lewis *et al.* [97]
^{64}Cu-ATSM					
^{64}Cu-ATSM					
^{64}Cu-ATSM	Hypoxia	Non-steady-state kinetic simulations	Oncology/EMT6 murine carcinoma	Mouse	Holland *et al.* [100]
^{61}Cu-ATSM	Hypoxia	Electrochemical model	Oncology/Head and neck cancer	Patient	Bowen *et al.* [101]
^{18}F-FMISO		Transformation function			
		pO$_2$ microelectrode			
^{64}Cu-ATSM	Hypoxia	Kinetic modeling	Oncology/Radiotherapy	Simulation work	Dalah *et al.* [102]
^{64}Cu-ATSM	Hypoxia	Dynamic PET	Oncology/Head and neck squamous cell carcinoma	Rat	McCall *et al.* [103]
		Autoradiography			
		Immunohistochemical staining			
^{62}Cu-PTSM	Hypoxia, perfusion	Dynamic PET	Multiple tracer protocol	Simulation work	Rust *et al.* [104]
^{62}Cu-ATSM		^{62}Cu-ATSM			
^{62}Cu-PTSM	Hypoxia, perfusion	Dynamic PET	Multiple tracer protocol	Dog	Black *et al.* [105]
^{62}Cu-ATSM		Compartment analysis	Signal separation and recovery		
^{18}F-FDG	Hypoxia, perfusion and glycolysis	Dynamic PET	Multiple tracer protocol	Dog	Black *et al.* [106]
^{62}Cu-PTSM		Compartment analysis	Signal separation and recovery		
^{62}Cu-ATSM					

blood time active concentration and can be obtained either by blood sampling or noninvasively from the left ventricle or large vessels by an image derived approach [89, 113, 114]. When using arterial blood sampling the input function should be corrected for dispersion and delay. On the other hand, for the non-invasive method a number of artifacts such as partial volume effect and respiratory movements can lead to misinterpretation [115]. Additionally, correction for plasma binding and metabolites should be considered.

Besides the technical aspects of kinetic modeling of dynamic PET data there are also factors more specific related to hypoxia imaging that needs to be considered. The hypoxia tracers that have been applied in dynamic PET imaging are lipophilic compounds that enter cells by free diffusion, become metabolized and consequently trapped within the cell. Based on the proposed trapping mechanisms of used hypoxia-specific tracers it is therefore reasonable to assume that they will be unable to leave the cell for the duration of the PET acquisition. On this basis, an irreversible model will be most suitable to reflect tracer accumulation *in vivo*. However, in studies comparing different compartment models for FAZA PET the difference between reversible and irreversible two compartment models were negligible [88, 89]. Importantly, recent studies have suggested that Cu-ATSM accumulation can perhaps be influenced by copper metabolism and that there can also be an efflux of Cu-ATSM or the radioactive copper from cells [116, 117], which should be kept in mind when applying kinetic models to dynamic Cu-ATSM PET data.

The majority of studies on kinetic modeling of hypoxia PET tracers are focused on cancer. As previously mentioned perfusion limited (acute) hypoxia is caused by changes in local tumor blood flow, and regional oxygenation can therefore suddenly change. These fluctuations represent a challenge, as the estimated parameters could be average values of varying oxygenation during the dynamic PET acquisition. In order to implement the use of kinetic models in clinic, the reproducibility of model output is an important part of the validation process. The reproducibility of model parameters derived from dynamic ^{18}F-FMISO PET has been investigated and some degree of variations was observed [66]. However, part of this variation could be

due to the fluctuating nature of acute hypoxia that influence tracer uptake and potentially also impact model parameters. Moreover, because hypoxia is a heterogeneous phenomenon with microregional differences in oxygen tension within a target tissue. This represents a challenge for quantification of PET imaging as uptake in a VOI will represent an average value with contribution from multiple microregions. This will also be reflected in the parameters estimated based on TACs generated from these VOIs. As an alternative, voxel-based tracer kinetic modeling can be applied and more precisely reflects the tracer behavior in smaller subvolumes [70, 118]. However, computation time for this approach is demanding, and the error scale will be much higher, compared to parameters calculated based on TACs derived from larger VOIs. Therefore it is important to get a reasonable balance between the signal to noise ratio and the definition of voxel size and frame duration. Increasing the injected dose can be a way to improve the signal to noise ratio but this will also increase the absorbed dose and should therefore be considered with caution.

Conclusion and future perspectives

Dynamic PET based kinetic modeling represents a methodology that can potentially be used to extract additional information of cellular processes. Despite some promising results, a number of technical difficulties and limitations need to be solved for clinical implementation, e.g. the limited field of view in clinical PET scanners, and development of methods for robust determination of the input function without continuous blood sampling. Several studies have shown that it is possible to obtain kinetic parameters from dynamic hypoxia PET data but at present validation of model output against other modalities is sparse. This review points out the potential applications of dynamic hypoxia PET imaging but before a kinetic model can be fully integrated in the clinic it needs to be validated and shown that it contributes to the current assessment routine.

Disclosure of conflict of interest

None.

Address correspondence to: Fan Li, Cluster for Molecular Imaging, Faculty of Health Sciences, University of Copenhagen, Blegdamsvej 3B, 2200

Copenhagen N, Denmark. Tel: +45 35326007; Fax: +45 35327248; E-mail: fanli@sund.ku.dk

References

[1] Hockel M and Vaupel P. Tumor hypoxia: definitions and current clinical, biologic, and molecular aspects. J Natl Cancer Inst 2001; 93: 266-276.

[2] Vaupel P and Harrison L. Tumor hypoxia: causative factors, compensatory mechanisms, and cellular response. Oncologist 2004; 9 Suppl 5: 4-9.

[3] Hockel M, Schlenger K, Mitze M, Schaffer U and Vaupel P. Hypoxia and Radiation Response in Human Tumors. Semin Radiat Oncol 1996; 6: 3-9.

[4] Brizel DM, Sibley GS, Prosnitz LR, Scher RL and Dewhirst MW. Tumor hypoxia adversely affects the prognosis of carcinoma of the head and neck. Int J Radiat Oncol Biol Phys 1997; 38: 285-289.

[5] Nordsmark M, Hoyer M, Keller J, Nielsen OS, Jensen OM and Overgaard J. The relationship between tumor oxygenation and cell proliferation in human soft tissue sarcomas. Int J Radiat Oncol Biol Phys 1996; 35: 701-708.

[6] Gray LH, Conger AD, Ebert M, Hornsey S and Scott OC. The concentration of oxygen dissolved in tissues at the time of irradiation as a factor in radiotherapy. Br J Radiol 1953; 26: 638-648.

[7] Brizel DM, Dodge RK, Clough RW and Dewhirst MW. Oxygenation of head and neck cancer: changes during radiotherapy and impact on treatment outcome. Radiother Oncol 1999; 53: 113-117.

[8] Huang SC, Williams BA, Krivokapich J, Araujo L, Phelps ME and Schelbert HR. Rabbit myocardial 82Rb kinetics and a compartmental model for blood flow estimation. Am J Physiol 1989; 256: H1156-1164.

[9] Tredan O, Galmarini CM, Patel K and Tannock IF. Drug resistance and the solid tumor microenvironment. J Natl Cancer Inst 2007; 99: 1441-1454.

[10] Skov KA and MacPhail S. Low concentrations of nitroimidazoles: effective radiosensitizers at low doses. Int J Radiat Oncol Biol Phys 1994; 29: 87-93.

[11] Lee DJ, Moini M, Giuliano J and Westra WH. Hypoxic sensitizer and cytotoxin for head and neck cancer. Ann Acad Med Singapore 1996; 25: 397-404.

[12] Kaanders JH, Bussink J and van der Kogel AJ. ARCON: a novel biology-based approach in radiotherapy. Lancet Oncol 2002; 3: 728-737.

[13] Jonathan RA, Wijffels KI, Peeters W, de Wilde PC, Marres HA, Merkx MA, Oosterwijk E, van der Kogel AJ and Kaanders JH. The prognostic value of endogenous hypoxia-related markers for head and neck squamous cell carcinomas treated with ARCON. Radiother Oncol 2006; 79: 288-297.

[14] Bernier J, Denekamp J, Rojas A, Trovo M, Horiot JC, Hamers H, Antognoni P, Dahl O, Richaud P, Kaanders J, van Glabbeke M and Pierart M. ARCON: accelerated radiotherapy with carbogen and nicotinamide in non small cell lung cancer: a phase I/II study by the EORTC. Radiother Oncol 1999; 52: 149-156.

[15] Loeffler JS and Durante M. Charged particle therapy--optimization, challenges and future directions. Nat Rev Clin Oncol 2013; 10: 411-424.

[16] Brurberg KG, Thuen M, Ruud EB and Rofstad EK. Fluctuations in pO2 in irradiated human melanoma xenografts. Radiat Res 2006; 165: 16-25.

[17] Brurberg KG, Skogmo HK, Graff BA, Olsen DR and Rofstad EK. Fluctuations in pO2 in poorly and well-oxygenated spontaneous canine tumors before and during fractionated radiation therapy. Radiother Oncol 2005; 77: 220-226.

[18] Vaupel P, Schlenger K, Knoop C and Hockel M. Oxygenation of human tumors: evaluation of tissue oxygen distribution in breast cancers by computerized O2 tension measurements. Cancer Res 1991; 51: 3316-3322.

[19] Brizel DM, Scully SP, Harrelson JM, Layfield LJ, Bean JM, Prosnitz LR and Dewhirst MW. Tumor oxygenation predicts for the likelihood of distant metastases in human soft tissue sarcoma. Cancer Res 1996; 56: 941-943.

[20] Nordsmark M, Bentzen SM, Rudat V, Brizel D, Lartigau E, Stadler P, Becker A, Adam M, Molls M, Dunst J, Terris DJ and Overgaard J. Prognostic value of tumor oxygenation in 397 head and neck tumors after primary radiation therapy. An international multi-center study. Radiother Oncol 2005; 77: 18-24.

[21] Griffiths JR and Robinson SP. The OxyLite: a fibre-optic oxygen sensor. Br J Radiol 1999; 72: 627-630.

[22] Tran LB, Bol A, Labar D, Jordan B, Magat J, Mignion L, Gregoire V and Gallez B. Hypoxia imaging with the nitroimidazole 18F-FAZA PET tracer: a comparison with OxyLite, EPR oximetry and 19F-MRI relaxometry. Radiother Oncol 2012; 105: 29-35.

[23] Bartlett RM, Beattie BJ, Naryanan M, Georgi JC, Chen Q, Carlin SD, Roble G, Zanzonico PB, Gonen M, O'Donoghue J, Fischer A and Humm JL. Image-guided PO2 probe measurements correlated with parametric images derived from 18F-fluoromisonidazole small-animal PET data in rats. J Nucl Med 2012; 53: 1608-1615.

[24] Kizaka-Kondoh S and Konse-Nagasawa H. Significance of nitroimidazole compounds and

hypoxia-inducible factor-1 for imaging tumor hypoxia. Cancer Sci 2009; 100: 1366-1373.

[25] Muzic RF Jr and Christian BT. Evaluation of objective functions for estimation of kinetic parameters. Med Phys 2006; 33: 342-353.

[26] Nitzsche EU, Choi Y, Czernin J, Hoh CK, Huang SC and Schelbert HR. Noninvasive quantification of myocardial blood flow in humans. A direct comparison of the [13N]ammonia and the [15O]water techniques. Circulation 1996; 93: 2000-2006.

[27] Rijpkema M, Schuuring J, Bernsen PL, Bernsen HJ, Kaanders JH, van der Kogel AJ and Heerschap A. BOLD MRI response to hypercapnic hyperoxia in patients with meningiomas: correlation with Gadolinium-DTPA uptake rate. Magn Reson Imaging 2004; 22: 761-767.

[28] Remmele S, Dahnke H, Flacke S, Soehle M, Wenningmann I, Kovacs A, Traber F, Muller A, Willinek WA, Konig R, Clusmann H, Gieseke J, Schild HH and Murtz P. Quantification of the magnetic resonance signal response to dynamic (C)O(2)-enhanced imaging in the brain at 3 T: R*(2) BOLD vs. balanced SSFP. J Magn Reson Imaging 2010; 31: 1300-1310.

[29] Yasui H, Matsumoto S, Devasahayam N, Munasinghe JP, Choudhuri R, Saito K, Subramanian S, Mitchell JB and Krishna MC. Low-field magnetic resonance imaging to visualize chronic and cycling hypoxia in tumor-bearing mice. Cancer Res 2010; 70: 6427-6436.

[30] Bobko AA, Dhimitruka I, Eubank TD, Marsh CB, Zweier JL and Khramtsov VV. Trityl-based EPR probe with enhanced sensitivity to oxygen. Free Radic Biol Med 2009; 47: 654-658.

[31] Reivich M, Kuhl D, Wolf A, Greenberg J, Phelps M, Ido T, Casella V, Fowler J, Gallagher B, Hoffman E, Alavi A and Sokoloff L. Measurement of local cerebral glucose metabolism in man with 18F-2-fluoro-2-deoxy-d-glucose. Acta Neurol Scand Suppl 1977; 64: 190-191.

[32] Bomanji JB, Costa DC and Ell PJ. Clinical role of positron emission tomography in oncology. Lancet Oncol 2001; 2: 157-164.

[33] Wang GL, Jiang BH, Rue EA and Semenza GL. Hypoxia-inducible factor 1 is a basic-helix-loop-helix-PAS heterodimer regulated by cellular O2 tension. Proc Natl Acad Sci U S A 1995; 92: 5510-5514.

[34] Zimny M, Gagel B, DiMartino E, Hamacher K, Coenen HH, Westhofen M, Eble M, Buell U and Reinartz P. FDG--a marker of tumour hypoxia? A comparison with [18F]fluoromisonidazole and pO2-polarography in metastatic head and neck cancer. Eur J Nucl Med Mol Imaging 2006; 33: 1426-1431.

[35] Cherk MH, Foo SS, Poon AM, Knight SR, Murone C, Papenfuss AT, Sachinidis JI, Saunder TH, O'Keefe GJ and Scott AM. Lack of correlation of hypoxic cell fraction and angiogenesis with glucose metabolic rate in non-small cell lung cancer assessed by 18F-Fluoromisonidazole and 18F-FDG PET. J Nucl Med 2006; 47: 1921-1926.

[36] Dierckx RA and Van de Wiele C. FDG uptake, a surrogate of tumour hypoxia? Eur J Nucl Med Mol Imaging 2008; 35: 1544-1549.

[37] Gagel B, Reinartz P, Dimartino E, Zimny M, Pinkawa M, Maneschi P, Stanzel S, Hamacher K, Coenen HH, Westhofen M, Bull U and Eble MJ. pO(2) Polarography versus positron emission tomography ([(18)F] fluoromisonidazole, [(18)F]-2-fluoro-2'-deoxyglucose). An appraisal of radiotherapeutically relevant hypoxia. Strahlenther Onkol 2004; 180: 616-622.

[38] Bentzen L, Keiding S, Horsman MR, Falborg L, Hansen SB and Overgaard J. Feasibility of detecting hypoxia in experimental mouse tumours with 18F-fluorinated tracers and positron emission tomography--a study evaluating [18F]Fluoro-2-deoxy-D-glucose. Acta Oncol 2000; 39: 629-637.

[39] Pugachev A, Ruan S, Carlin S, Larson SM, Campa J, Ling CC and Humm JL. Dependence of FDG uptake on tumor microenvironment. Int J Radiat Oncol Biol Phys 2005; 62: 545-553.

[40] Willemsen AT and van den Hoff J. Fundamentals of quantitative PET data analysis. Curr Pharm Des 2002; 8: 1513-1526.

[41] Eschmann SM, Paulsen F, Reimold M, Dittmann H, Welz S, Reischl G, Machulla HJ and Bares R. Prognostic impact of hypoxia imaging with 18F-misonidazole PET in non-small cell lung cancer and head and neck cancer before radiotherapy. J Nucl Med 2005; 46: 253-260.

[42] Thorwarth D, Eschmann SM, Scheiderbauer J, Paulsen F and Alber M. Kinetic analysis of dynamic 18F-fluoromisonidazole PET correlates with radiation treatment outcome in head-and-neck cancer. BMC Cancer 2005; 5: 152.

[43] Gunn RN, Gunn SR, Turkheimer FE, Aston JA and Cunningham VJ. Positron emission tomography compartmental models: a basis pursuit strategy for kinetic modeling. J Cereb Blood Flow Metab 2002; 22: 1425-1439.

[44] Dolbier WR Jr, Li AR, Koch CJ, Shiue CY and Kachur AV. [18F]-EF5, a marker for PET detection of hypoxia: synthesis of precursor and a new fluorination procedure. Appl Radiat Isot 2001; 54: 73-80.

[45] Rijpkema M, Kaanders JH, Joosten FB, van der Kogel AJ and Heerschap A. Method for quantitative mapping of dynamic MRI contrast agent uptake in human tumors. J Magn Reson Imaging 2001; 14: 457-463.

[46] Tofts PS, Brix G, Buckley DL, Evelhoch JL, Henderson E, Knopp MV, Larsson HB, Lee TY, Mayr NA, Parker GJ, Port RE, Taylor J and Weisskoff

RM. Estimating kinetic parameters from dynamic contrast-enhanced T(1)-weighted MRI of a diffusable tracer: standardized quantities and symbols. J Magn Reson Imaging 1999; 10: 223-232.

[47] Phelps M. PET: Molecular Imaging and Its Biological Applications. New York: Springer; 2004.

[48] Takesh M. The Potential Benefit by Application of Kinetic Analysis of PET in the Clinical Oncology. ISRN Oncol 2012; 2012: 349351.

[49] Kadrmas DJ and Oktay MB. Generalized separable parameter space techniques for fitting 1K-5K serial compartment models. Med Phys 2013; 40: 072502.

[50] Logan J, Fowler JS, Volkow ND, Wolf AP, Dewey SL, Schlyer DJ, MacGregor RR, Hitzemann R, Bendriem B, Gatley SJ, et al. Graphical analysis of reversible radioligand binding from time-activity measurements applied to [N-11C-methyl]-(-)-cocaine PET studies in human subjects. J Cereb Blood Flow Metab 1990; 10: 740-747.

[51] Kaanders JH, Wijffels KI, Marres HA, Ljungkvist AS, Pop LA, van den Hoogen FJ, de Wilde PC, Bussink J, Raleigh JA and van der Kogel AJ. Pimonidazole binding and tumor vascularity predict for treatment outcome in head and neck cancer. Cancer Res 2002; 62: 7066-7074.

[52] Olive PL, Durand RE, Raleigh JA, Luo C and Aquino-Parsons C. Comparison between the comet assay and pimonidazole binding for measuring tumour hypoxia. Br J Cancer 2000; 83: 1525-1531.

[53] Raleigh JA, Chou SC, Arteel GE and Horsman MR. Comparisons among pimonidazole binding, oxygen electrode measurements, and radiation response in C3H mouse tumors. Radiat Res 1999; 151: 580-589.

[54] Chang Q, Jurisica I, Do T and Hedley DW. Hypoxia predicts aggressive growth and spontaneous metastasis formation from orthotopically grown primary xenografts of human pancreatic cancer. Cancer Res 2011; 71: 3110-3120.

[55] Andreyev A and Celler A. Dual-isotope PET using positron-gamma emitters. Phys Med Biol 2011; 56: 4539-4556.

[56] Chapman JD, Baer K and Lee J. Characteristics of the metabolism-induced binding of misonidazole to hypoxic mammalian cells. Cancer Res 1983; 43: 1523-1528.

[57] Chapman JD, Franko AJ and Sharplin J. A marker for hypoxic cells in tumours with potential clinical applicability. Br J Cancer 1981; 43: 546-550.

[58] Rasey JS, Koh WJ, Grierson JR, Grunbaum Z and Krohn KA. Radiolabelled fluoromisonidazole as an imaging agent for tumor hypoxia. Int J Radiat Oncol Biol Phys 1989; 17: 985-991.

[59] Boellaard R, Knaapen P, Rijbroek A, Luurtsema GJ and Lammertsma AA. Evaluation of basis function and linear least squares methods for generating parametric blood flow images using 15O-water and Positron Emission Tomography. Mol Imaging Biol 2005; 7: 273-285.

[60] Valk PE, Mathis CA, Prados MD, Gilbert JC and Budinger TF. Hypoxia in human gliomas: demonstration by PET with fluorine-18-fluoromisonidazole. J Nucl Med 1992; 33: 2133-2137.

[61] Spence AM, Muzi M, Swanson KR, O'Sullivan F, Rockhill JK, Rajendran JG, Adamsen TC, Link JM, Swanson PE, Yagle KJ, Rostomily RC, Silbergeld DL and Krohn KA. Regional hypoxia in glioblastoma multiforme quantified with [18F] fluoromisonidazole positron emission tomography before radiotherapy: correlation with time to progression and survival. Clin Cancer Res 2008; 14: 2623-2630.

[62] Bentzen L, Keiding S, Nordsmark M, Falborg L, Hansen SB, Keller J, Nielsen OS and Overgaard J. Tumour oxygenation assessed by 18F-fluoromisonidazole PET and polarographic needle electrodes in human soft tissue tumours. Radiother Oncol 2003; 67: 339-344.

[63] Rasey JS, Casciari JJ, Hofstrand PD, Muzi M, Graham MM and Chin LK. Determining hypoxic fraction in a rat glioma by uptake of radiolabeled fluoromisonidazole. Radiat Res 2000; 153: 84-92.

[64] Casciari JJ, Graham MM and Rasey JS. A modeling approach for quantifying tumor hypoxia with [F-18]fluoromisonidazole PET time-activity data. Med Phys 1995; 22: 1127-1139.

[65] Kelly CJ and Brady M. A model to simulate tumour oxygenation and dynamic [18F]-Fmiso PET data. Phys Med Biol 2006; 51: 5859-5873.

[66] Whisenant JG, Peterson TE, Fluckiger JU, Tantawy MN, Ayers GD and Yankeelov TE. Reproducibility of static and dynamic (18)F-FDG, (18)F-FLT, and (18)F-FMISO MicroPET studies in a murine model of HER2+ breast cancer. Mol Imaging Biol 2013; 15: 87-96.

[67] Bejot R, Kersemans V, Kelly C, Carroll L, King RC, Gouverneur V, Elizarov AM, Ball C, Zhang J, Miraghaie R, Kolb HC, Smart S and Hill S. Preclinical evaluation of a 3-nitro-1,2,4-triazole analogue of [18F]FMISO as hypoxia-selective tracer for PET. Nucl Med Biol 2010; 37: 565-575.

[68] Bruehlmeier M, Roelcke U, Schubiger PA and Ametamey SM. Assessment of hypoxia and perfusion in human brain tumors using PET with 18F-fluoromisonidazole and 15O-H2O. J Nucl Med 2004; 45: 1851-1859.

[69] Bruehlmeier M, Kaser-Hotz B, Achermann R, Bley CR, Wergin M, Schubiger PA and Ametamey SM. Measurement of tumor hypoxia in

spontaneous canine sarcomas. Vet Radiol Ultrasound 2005; 46: 348-354.

[70] Thorwarth D, Eschmann SM, Paulsen F and Alber M. A kinetic model for dynamic [18F]-Fmiso PET data to analyse tumour hypoxia. Phys Med Biol 2005; 50: 2209-2224.

[71] Cho H, Ackerstaff E, Carlin S, Lupu ME, Wang Y, Rizwan A, O'Donoghue J, Ling CC, Humm JL, Zanzonico PB and Koutcher JA. Noninvasive multimodality imaging of the tumor microenvironment: registered dynamic magnetic resonance imaging and positron emission tomography studies of a preclinical tumor model of tumor hypoxia. Neoplasia 2009; 11: 247-259, 242p following 259.

[72] Wang W, Georgi JC, Nehmeh SA, Narayanan M, Paulus T, Bal M, O'Donoghue J, Zanzonico PB, Schmidtlein CR, Lee NY and Humm JL. Evaluation of a compartmental model for estimating tumor hypoxia via FMISO dynamic PET imaging. Phys Med Biol 2009; 54: 3083-3099.

[73] Wang W, Lee NY, Georgi JC, Narayanan M, Guillem J, Schoder H and Humm JL. Pharmacokinetic analysis of hypoxia (18)F-fluoromisonidazole dynamic PET in head and neck cancer. J Nucl Med 2010; 51: 37-45.

[74] Takasawa M, Beech JS, Fryer TD, Hong YT, Hughes JL, Igase K, Jones PS, Smith R, Aigbirhio FI, Menon DK, Clark JC and Baron JC. Imaging of brain hypoxia in permanent and temporary middle cerebral artery occlusion in the rat using 18F-fluoromisonidazole and positron emission tomography: a pilot study. J Cereb Blood Flow Metab 2007; 27: 679-689.

[75] Hong YT, Beech JS, Smith R, Baron JC and Fryer TD. Parametric mapping of [18F]fluoromisonidazole positron emission tomography using basis functions. J Cereb Blood Flow Metab 2011; 31: 648-657.

[76] Nunn A, Linder K and Strauss HW. Nitroimidazoles and imaging hypoxia. Eur J Nucl Med 1995; 22: 265-280.

[77] Yang DJ, Wallace S, Cherif A, Li C, Gretzer MB, Kim EE and Podoloff DA. Development of F-18-labeled fluoroerythronitroimidazole as a PET agent for imaging tumor hypoxia. Radiology 1995; 194: 795-800.

[78] van Loon J, Janssen MH, Ollers M, Aerts HJ, Dubois L, Hochstenbag M, Dingemans AM, Lalisang R, Brans B, Windhorst B, van Dongen GA, Kolb H, Zhang J, De Ruysscher D and Lambin P. PET imaging of hypoxia using [18F]HX4: a phase I trial. Eur J Nucl Med Mol Imaging 2010; 37: 1663-1668.

[79] Vercellino L, Groheux D, Thoury A, Delord M, Schlageter MH, Delpech Y, Barre E, Baruch-Hennequin V, Tylski P, Homyrda L, Walker F, Barranger E and Hindie E. Hypoxia imaging of uterine cervix carcinoma with (18)F-FETNIM PET/CT. Clin Nucl Med 2012; 37: 1065-1068.

[80] Lehtio K, Oikonen V, Nyman S, Gronroos T, Roivainen A, Eskola O and Minn H. Quantifying tumour hypoxia with fluorine-18 fluoroerythronitroimidazole ([18F]FETNIM) and PET using the tumour to plasma ratio. Eur J Nucl Med Mol Imaging 2003; 30: 101-108.

[81] Lehtio K, Oikonen V, Gronroos T, Eskola O, Kalliokoski K, Bergman J, Solin O, Grenman R, Nuutila P and Minn H. Imaging of blood flow and hypoxia in head and neck cancer: initial evaluation with [(15)O]H(2)O and [(18)F]fluoroerythronitroimidazole PET. J Nucl Med 2001; 42: 1643-1652.

[82] Kumar P, Wiebe LI, Asikoglu M, Tandon M and McEwan AJ. Microwave-assisted (radio)halogenation of nitroimidazole-based hypoxia markers. Appl Radiat Isot 2002; 57: 697-703.

[83] Piert M, Machulla HJ, Picchio M, Reischl G, Ziegler S, Kumar P, Wester HJ, Beck R, McEwan AJ, Wiebe LI and Schwaiger M. Hypoxia-specific tumor imaging with 18F-fluoroazomycin arabinoside. J Nucl Med 2005; 46: 106-113.

[84] Sorger D, Patt M, Kumar P, Wiebe LI, Barthel H, Seese A, Dannenberg C, Tannapfel A, Kluge R and Sabri O. [18F]Fluoroazomycinarabinofuranoside (18FAZA) and [18F]Fluoromisonidazole (18FMISO): a comparative study of their selective uptake in hypoxic cells and PET imaging in experimental rat tumors. Nucl Med Biol 2003; 30: 317-326.

[85] Postema EJ, McEwan AJ, Riauka TA, Kumar P, Richmond DA, Abrams DN and Wiebe LI. Initial results of hypoxia imaging using 1-alpha-D:-(5-deoxy-5-[18F]-fluoroarabinofuranosyl)-2-nitroimidazole (18F-FAZA). Eur J Nucl Med Mol Imaging 2009; 36: 1565-1573.

[86] Reischl G, Dorow DS, Cullinane C, Katsifis A, Roselt P, Binns D and Hicks RJ. Imaging of tumor hypoxia with [124I]IAZA in comparison with [18F]FMISO and [18F]FAZA--first small animal PET results. J Pharm Pharm Sci 2007; 10: 203-211.

[87] Busk M, Munk OL, Jakobsen S, Wang T, Skals M, Steiniche T, Horsman MR and Overgaard J. Assessing hypoxia in animal tumor models based on pharmocokinetic analysis of dynamic FAZA PET. Acta Oncol 2010; 49: 922-933.

[88] Shi K, Souvatzoglou M, Astner ST, Vaupel P, Nusslin F, Wilkens JJ and Ziegler SI. Quantitative assessment of hypoxia kinetic models by a cross-study of dynamic 18F-FAZA and 15O-H2O in patients with head and neck tumors. J Nucl Med 2010; 51: 1386-1394.

[89] Verwer EE, van Velden FH, Bahce I, Yaqub M, Schuit RC, Windhorst AD, Raijmakers P, Lammertsma AA, Smit EF and Boellaard R. Pharmacokinetic analysis of [18F]FAZA in non-small cell lung cancer patients. Eur J Nucl Med Mol Imaging 2013; 40: 1523-1531.

[90] Fujibayashi Y, Taniuchi H, Yonekura Y, Ohtani H, Konishi J and Yokoyama A. Copper-62-ATSM: a new hypoxia imaging agent with high membrane permeability and low redox potential. J Nucl Med 1997; 38: 1155-1160.

[91] Dehdashti F, Mintun MA, Lewis JS, Bradley J, Govindan R, Laforest R, Welch MJ and Siegel BA. In vivo assessment of tumor hypoxia in lung cancer with 60Cu-ATSM. Eur J Nucl Med Mol Imaging 2003; 30: 844-850.

[92] Dehdashti F, Grigsby PW, Lewis JS, Laforest R, Siegel BA and Welch MJ. Assessing tumor hypoxia in cervical cancer by PET with 60Cu-labeled diacetyl-bis(N4-methylthiosemicarbazone). J Nucl Med 2008; 49: 201-205.

[93] Dietz DW, Dehdashti F, Grigsby PW, Malyapa RS, Myerson RJ, Picus J, Ritter J, Lewis JS, Welch MJ and Siegel BA. Tumor hypoxia detected by positron emission tomography with 60Cu-ATSM as a predictor of response and survival in patients undergoing Neoadjuvant chemoradiotherapy for rectal carcinoma: a pilot study. Dis Colon Rectum 2008; 51: 1641-1648.

[94] Yuan H, Schroeder T, Bowsher JE, Hedlund LW, Wong T and Dewhirst MW. Intertumoral differences in hypoxia selectivity of the PET imaging agent 64Cu(II)-diacetyl-bis(N4-methylthiosemicarbazone). J Nucl Med 2006; 47: 989-998.

[95] O'Donoghue JA, Zanzonico P, Pugachev A, Wen B, Smith-Jones P, Cai S, Burnazi E, Finn RD, Burgman P, Ruan S, Lewis JS, Welch MJ, Ling CC and Humm JL. Assessment of regional tumor hypoxia using 18F-fluoromisonidazole and 64Cu(II)-diacetyl-bis(N4-methylthiosemicarbazone) positron emission tomography: Comparative study featuring microPET imaging, Po2 probe measurement, autoradiography, and fluorescent microscopy in the R3327-AT and FaDu rat tumor models. Int J Radiat Oncol Biol Phys 2005; 61: 1493-1502.

[96] Lewis JS, McCarthy DW, McCarthy TJ, Fujibayashi Y and Welch MJ. Evaluation of 64Cu-ATSM in vitro and in vivo in a hypoxic tumor model. J Nucl Med 1999; 40: 177-183.

[97] Lewis JS, Herrero P, Sharp TL, Engelbach JA, Fujibayashi Y, Laforest R, Kovacs A, Gropler RJ and Welch MJ. Delineation of hypoxia in canine myocardium using PET and copper(II)-diacetyl-bis(N(4)-methylthiosemicarbazone). J Nucl Med 2002; 43: 1557-1569.

[98] Dearling JL and Packard AB. Some thoughts on the mechanism of cellular trapping of Cu(II)-ATSM. Nucl Med Biol 2010; 37: 237-243.

[99] Burgman P, O'Donoghue JA, Lewis JS, Welch MJ, Humm JL and Ling CC. Cell line-dependent differences in uptake and retention of the hypoxia-selective nuclear imaging agent Cu-ATSM. Nucl Med Biol 2005; 32: 623-630.

[100] Holland JP, Giansiracusa JH, Bell SG, Wong LL and Dilworth JR. In vitro kinetic studies on the mechanism of oxygen-dependent cellular uptake of copper radiopharmaceuticals. Phys Med Biol 2009; 54: 2103-2119.

[101] Bowen SR, van der Kogel AJ, Nordsmark M, Bentzen SM and Jeraj R. Characterization of positron emission tomography hypoxia tracer uptake and tissue oxygenation via electrochemical modeling. Nucl Med Biol 2011; 38: 771-780.

[102] Dalah E, Bradley D and Nisbet A. Simulation of tissue activity curves of (64)Cu-ATSM for subtarget volume delineation in radiotherapy. Phys Med Biol 2010; 55: 681-694.

[103] McCall KC, Humm JL, Bartlett R, Reese M and Carlin S. Copper-64-diacetyl-bis(N(4)-methylthiosemicarbazone) pharmacokinetics in FaDu xenograft tumors and correlation with microscopic markers of hypoxia. Int J Radiat Oncol Biol Phys 2012; 84: e393-399.

[104] Rust TC and Kadrmas DJ. Rapid dual-tracer PTSM+ATSM PET imaging of tumour blood flow and hypoxia: a simulation study. Phys Med Biol 2006; 51: 61-75.

[105] Black NF, McJames S, Rust TC and Kadrmas DJ. Evaluation of rapid dual-tracer (62)Cu-PTSM + (62)Cu-ATSM PET in dogs with spontaneously occurring tumors. Phys Med Biol 2008; 53: 217-232.

[106] Black NF, McJames S and Kadrmas DJ. Rapid Multi-Tracer PET Tumor Imaging With F-FDG and Secondary Shorter-Lived Tracers. IEEE Trans Nucl Sci 2009; 56: 2750-2758.

[107] Ikoma Y, Watabe H, Shidahara M, Naganawa M and Kimura Y. PET kinetic analysis: error consideration of quantitative analysis in dynamic studies. Ann Nucl Med 2008; 22: 1-11.

[108] Wu FX and Mu L. Parameter estimation in rational models of molecular biological systems. Conf Proc IEEE Eng Med Biol Soc 2009; 2009: 3263-3266.

[109] Luenberger D. Optimization by vector space methods. New York: Wiley; 1969.

[110] Marquardt D. An algorithm for least squares estimation of nonlinear parameters. SIAM J Soc Ind Appl Math 1963; 11: 431-441.

[111] Dai X, Chen Z and Tian J. Performance evaluation of kinetic parameter estimation methods in dynamic FDG-PET studies. Nucl Med Commun 2011; 32: 4-16.

[112] Croteau E, Lavallee E, Labbe SM, Hubert L, Pifferi F, Rousseau JA, Cunnane SC, Carpentier AC, Lecomte R and Benard F. Image-derived input function in dynamic human PET/CT: methodology and validation with 11C-acetate and 18F-fluorothioheptadecanoic acid in muscle and 18F-fluorodeoxyglucose in brain. Eur J Nucl Med Mol Imaging 2010; 37: 1539-1550.

[113] Fang YH and Muzic RF Jr. Spillover and partial-volume correction for image-derived input functions for small-animal 18F-FDG PET studies. J Nucl Med 2008; 49: 606-614.

[114] Laforest R, Sharp TL, Engelbach JA, Fettig NM, Herrero P, Kim J, Lewis JS, Rowland DJ, Tai YC and Welch MJ. Measurement of input functions in rodents: challenges and solutions. Nucl Med Biol 2005; 32: 679-685.

[115] Zanotti-Fregonara P, Chen K, Liow JS, Fujita M and Innis RB. Image-derived input function for brain PET studies: many challenges and few opportunities. J Cereb Blood Flow Metab 2011; 31: 1986-1998.

[116] Hueting R, Kersemans V, Cornelissen B, Tredwell M, Hussien K, Christlieb M, Gee AD, Passchier J, Smart SC, Dilworth JR, Gouverneur V and Muschel RJ. A comparison of the behavior of (64)Cu-acetate and (64)Cu-ATSM in vitro and in vivo. J Nucl Med 2014; 55: 128-134.

[117] Liu J, Hajibeigi A, Ren G, Lin M, Siyambalapitiyage W, Liu Z, Simpson E, Parkey RW, Sun X and Oz OK. Retention of the radiotracers 64Cu-ATSM and 64Cu-PTSM in human and murine tumors is influenced by MDR1 protein expression. J Nucl Med 2009; 50: 1332-1339.

[118] El Fakhri G, Sitek A, Guerin B, Kijewski MF, Di Carli MF and Moore SC. Quantitative dynamic cardiac 82Rb PET using generalized factor and compartment analyses. J Nucl Med 2005; 46: 1264-1271.